Stability of amorphous Ta–O nanotubes prepared by anodization: Thermal and structural analyses

Ryusuke Nakamura[a)]
Department of Materials Science, Graduate School of Engineering, Osaka Prefecture University, Naka-ku, Sakai 599-8531, Japan

Kohta Asano
National Institute of Advanced Industrial Science and Technology (AIST), Tsukuba, Ibaraki 305-8565, Japan

Manabu Ishimaru
Department of Materials Science and Engineering, Kyushu Institute of Technology, Tobata, Kitakyushu, Fukuoka 804-8550, Japan

Kazuhisa Sato
Institute for Materials Research, Tohoku University, Sendai 980-8577, Japan

Masahide Takahashi and Hiroshi Numakura
Department of Materials Science, Graduate School of Engineering, Osaka Prefecture University, Sakai 599-8531, Japan

(Received 15 October 2013; accepted 19 February 2014)

Amorphous Ta–O nanotubes (NTs) prepared by anodization in a sulfuric-acid-based solution have been found to contain considerable amounts of extra oxygen and sulfur. Their structural and thermal stability has been studied by combining x-ray diffractometry, transmission electron microscopy, and thermal analysis. The amorphous Ta–O, whose composition was estimated to be $Ta_2O_{6.6}S_{0.7}$, crystallizes into orthorhombic β-Ta_2O_5 at temperatures around 1073 K by an endothermic reaction, at which excess oxygen and impurity sulfur are released. The amorphous NTs were found to be thermally more stable than stoichiometric amorphous Ta_2O_5, whose crystallization temperature is around 973 K. Excess oxygen and impurity sulfur, which form chemical bonds with Ta atoms in the amorphous solid, must be the origin of the stability. The crystallization follows the out-diffusion of oxygen and sulfur from the solid at temperatures where the mobility of atoms is high enough, indicating that the crystallization is kinetically arrested.

I. INTRODUCTION

Nanoporous oxides have attracted much attention as potentially useful materials for ion exchange, molecular separation, catalysis, chromatography, and energy storage, as the large surface-to-volume ratio is expected to improve performance pertinent to these characteristics.[1,2] Fabrication of highly ordered, self-organized nanoporous oxides has stimulated substantial research since Masuda et al.[3] reported hexagonally ordered porous alumina structures on Al surface in acidic solutions. Nowadays, electrochemical anodization is recognized as a useful technique to obtain a variety of self-organized nanoporous oxides on the surface of metals such as Ti,[4] Nb,[5] Zr,[6] Hf,[7] W,[8] and Ta.[9]

With its wide band gap, of 3.8–4.3 eV,[10] Ta_2O_5 is not advantageous for solar light-harvesting. However, modification with other oxides such as NiO and RuO_2 can improve its photocatalytic ability for water-splitting under UV irradiation.[11] In addition, providing a large surface area is also effective for the same purpose. It has stimulated attempts to render nanoporous structures to Ta_2O_5. Owing to recent developments in electrochemical anodization processing, it is now easy to obtain ordered arrays of nanotubes (NTs)[12,13] or free-standing NTs[14,15] of Ta_2O_5. The photocatalytic activity of Ta_2O_5 NTs for hydrogen production from a water/ethanol solution under UV irradiation has been evaluated.[15]

In general, anodized NTs are amorphous and post-annealing is required to obtain crystalline NTs, which are more useful in applications such as photocatalysis. Oxide NTs prepared in fluoride- and sulfide-containing electrolytes often contain fluorine and sulfur as impurities.[14,15] For example, Gonçalves et al.[15] prepared Ta–O NTs in an electrolytic solution of H_2SO_4 and HF electrolyte and found the product contained impurity sulfur and more oxygen than the stoichiometric composition, Ta_2O_5. As reported by Allam and El-Sayed,[16] furthermore, dopants and impurities from the electrolyte change the transition

[a)]Address all correspondence to this author.
e-mail: nakamura@mtr.osakafu-u.ac.jp
DOI: 10.1557/jmr.2014.44

 © Materials Research Society 2014

https://doi.org/10.1557/jmr.2014.44 Published online by Cambridge University Press

temperature of oxide NTs. Effects of extra atoms (including impurities) on the thermal stability of amorphous NTs are, therefore, worthy of investigation.

The crystallization temperature (T_x) of amorphous Ta–O has been reported by several researchers. T_x of Ta_2O_5 thin films prepared by sputtering a Ta_2O_5 crystalline target is above 973 K.[17] On the other hand, T_x for anodized Ta–O depends on the preparation condition. For amorphous NT arrays on a tantalum substrate prepared in H_2SO_4 + HF including some additives such as H_3PO_4, ethylene glycol, or dimethyl sulfoxide, it is in the range of 573–823 K.[12,13] For free-standing NTs prepared in a H_2SO_4-based electrolyte including a smaller amount of HF, on the other hand, it is above 1023 K.[14,15] The large discrepancy in T_x suggests that possibly external effects from a substrate may blind internal factors on thermal stability such as the effects of extra atoms included in amorphous NTs. To study the origin of the thermal stability of anodized NTs, therefore, free-standing NTs are convenient to use, because they are free from substrates. The roles of the extra atoms will be clarified by comparing the crystallization behavior of free-standing NTs and impurity-free amorphous Ta_2O_5 prepared by sputtering.

For this purpose, a combination of thermal analysis and structural analysis techniques was used in this work to quantitatively analyze thermal events caused by structural change and/or reaction. Furthermore, radial distribution function (RDF) analysis of the atomic structure by transmission electron microscopy (TEM), using nano-sized electron beam, was performed because it provides the information on chemical bonds of the amorphous solid with excess atoms.[18,19] Based on these analyses, we discussed the thermal stability of amorphous Ta–O NTs, focusing on the chemical bonds formed by extra atoms.

II. EXPERIMENTAL PROCEDURE

Amorphous tantalum oxide NTs were grown by electrochemical anodization of a 0.5-mm-thick tantalum sheet (99.9% purity, Nilaco, Tokyo, Japan) in a solution of H_2SO_4 + 1 vol% HF + 4 vol% H_2O (98% H_2SO_4, 48% HF, distilled water).[14,15] Tantalum and platinum sheets, both in 20 × 20 mm^2, were used as anode and counter electrode, respectively. They were spot-welded on a tantalum wire of 0.5 mm in diameter and 100 mm in length. Prior to anodization, the tantalum and platinum sheets were degreased by sonication in acetone and ethanol, followed by rinsing with distilled water. The anodization was performed under a constant voltage of 50 V for 1–10 h at room temperature, with the distance between the tantalum and platinum electrodes being maintained at 20 mm. Immediately after anodization, the tantalum sheet, on which an oxide layer was grown, was carefully immersed in distilled water. As reported by Gonçalves et al.,[15] the oxide NTs could be removed easily from the tantalum substrate; they were collected in the form of powder after rinsing carefully with distilled water.

Thermal analyses of the powders were performed by thermogravimetry-differential thermal analysis (TG-DTA) and differential scanning calorimetry (DSC) using Rigaku TG8120 (Tokyo, Japan) and Netzsch DSC404F3 (Selb, Germany), respectively. The former is equipped with a quadrupole mass spectrometer (M-QA100TS, Anelva, Kawasaki, Japan), which makes it possible to identify desorbed molecules. Measurements were carried out in a stream of argon in the temperature range between 300 and 1300 K with the heating and cooling rates of 3–30 K/min. Samples of around 20 mg and around 2 mg were subjected to the TG-DTA and DSC measurements, respectively.

The structure and morphology of as-anodized and annealed NTs were examined by x-ray diffractometry (XRD) and TEM. XRD profiles were measured using a Rigaku RINT 2500V (Tokyo, Japan) diffractometer with Cu K_α radiation over a 2θ range from 3° to 100°. The microstructure and composition were examined using a JEOL 3000F TEM (Tokyo, Japan) and a FEI Titan 80-300 TEM (Hillsboro, OR) equipped with an energy-dispersive x-ray spectrometer (EDS). To avoid contamination, electron diffraction intensities and EDS spectra were measured at a cryogenic temperature using a cooling holder. For the radial distribution function analysis of the amorphous structure, electron diffraction patterns from a single nanotube were recorded on an imaging plate (Eu^{2+}-doped BaFBr). The electron diffraction patterns were analyzed quantitatively using an imaging-plate processor (Digital Micro-Luminography FDL 5000 system, Fuji Film (Tokyo, Japan)).

III. RESULTS AND DISCUSSION

A. Structure and morphology

Figure 1 shows XRD profiles of as-anodized samples (a) and those heated up to 1058 K (b) and 1128 K (c) in an argon atmosphere. (The latter two are those used for the TG-DTA measurements (Sec. III. B), where the heat treatment was given.) The broad maxima around 30° and 54° in the profiles of as-anodized samples (a) and those annealed up to 1058 K (b) (in the lower frame) indicate that they are essentially amorphous. After annealing up to 1128 K (c) (in the upper frame), the amorphous oxide transformed into a crystalline phase. All the peaks, including small ones, are identified as those corresponding to the low temperature phase, orthorhombic β-Ta_2O_5[20]; the largest five peaks of them correspond to 100 (2θ = 22.9°), 0$\underline{1}$11 (28.4°), 1$\underline{1}$11 (36.8°), 200 (46.7°), and 2$\underline{1}$11 (55.5°). The crystallization behavior is in good agreement with the result by Gonçalves et al.[15] At temperatures below 1058 K, the amorphous structure was virtually maintained, although weak diffraction peaks corresponding to 100, 0$\underline{1}$11, and 1$\underline{1}$11 of β-Ta_2O_5 appeared, as indicated by arrows. It should be noted that the shape and intensity of

https://doi.org/10.1557/jmr.2014.44 Published online by Cambridge University Press

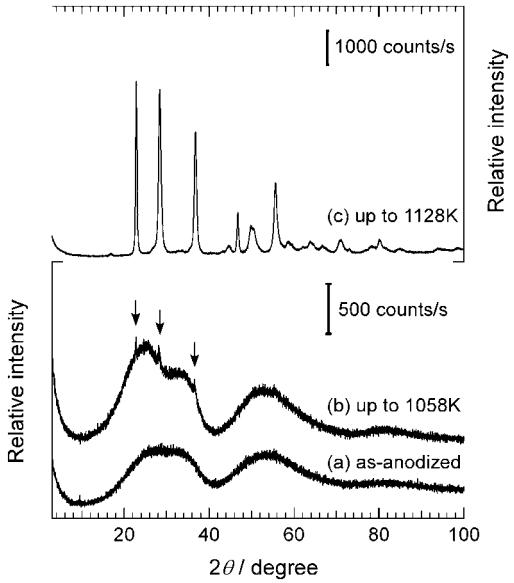


FIG. 1. XRD profiles of (a) as-anodized and (b, c) annealed Ta–O NTs: (b) up to 1058 K and (c) up to 1128 K.

the broad diffraction maxima around 30° in a profile (b) clearly differ from those in (a), suggesting that some changes occurred in the amorphous structure during the annealing. Detailed discussion is given in Sec. III. D on the basis of radial distribution function analyses.

Figure 2 shows bright-field electron-microscopy images and selected-area electron diffraction patterns of as-anodized samples (a, a'), and those annealed up to 1058 K (b, b') and 1128 K (c, c'). The as-prepared samples are amorphous and have uniform NT structures with inner and outer diameters of ~80 and ~170 nm, respectively. Samples annealed up to 1128 K (c, c') fully crystallized into Ta_2O_5 with nanosized grains, retaining the NT morphology.

Figure 3 shows a low-energy portion of characteristic x-ray spectra observed by TEM-EDS. The intensities are normalized to that of Ta M_α at around 1.75 keV. The characteristic x-rays of C and Cu come from contamination and from the grid, respectively. The S K_α peak was observed in (a) and (b), but not in (c). The intensity of S K_α peak is almost unchanged from (a) to (b), i.e., by annealing up to 1058 K. It is also the case for the O K_α peak. After annealing up to 1128 K (c), S K_α peak disappeared and the intensity of O K_α peak decreased, indicating that impurity sulfur and excess oxygen were released on crystallization. The presence and release of impurity sulfur and excess oxygen were also reported by Gonçalves et al.[15] Figure 4 shows intensity line-profiles of the characteristic x-rays of Ta, O, and S obtained across a single nanotube in (a) an as-anodized sample and (b) a sample annealed up to 1058 K. The position, $x = 0$, corresponds to the center of the nanotube, as shown in the corresponding BFI (a') to the profile (a). The arrow in (a') indicates a trace by beam-scanning. The thickness near the edges of the NTs is too small to

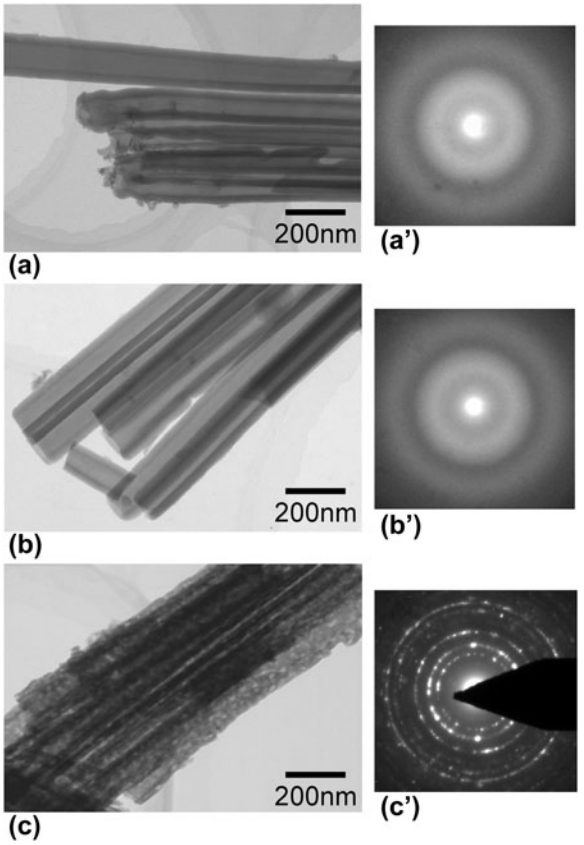


FIG. 2. Bright-field electron-microscopy images of as-anodized Ta–O NTs (a), and those annealed up to 1058 K (b) and 1128 K (c). (a'–c') The corresponding selected-area electron diffraction patterns.

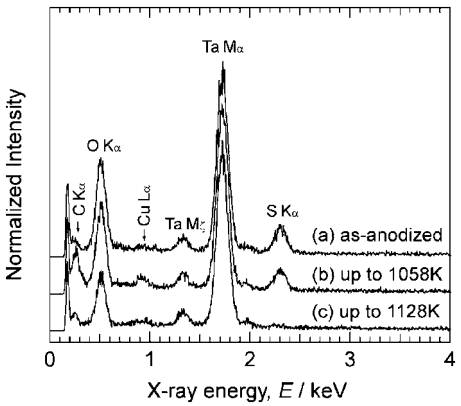


FIG. 3. Energy-dispersive x-ray spectra at lower energy region for the anodic Ta–O corresponding to Fig. 2. (a) As-anodized Ta–O NTs and those annealed (b) up to 1058 K and (c) 1128 K. These spectra are normalized to the peak height of Ta M_α.

detect sufficient x-ray intensity by line-scanning. The intensities of O K_α and S K_α lines normalized to that of Ta M_α except the edges are almost constant. The relative intensities of O K_α and S K_α to that of Ta M_α from an edge area were observed to be comparable to those from an entire nanotube. Therefore, oxygen and sulfur are not concentrated near the surfaces of a nanotube but distributed homogeneously.

https://doi.org/10.1557/jmr.2014.44 Published online by Cambridge University Press

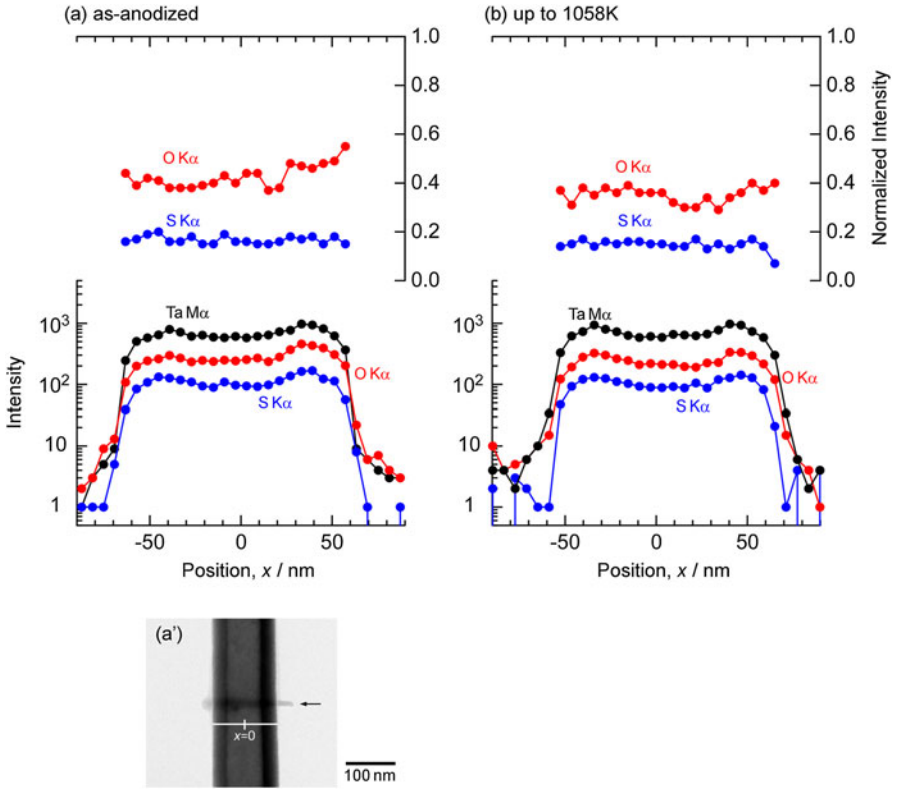


FIG. 4. Line-profiles of characteristic x-ray intensity obtained across a single nanotube of (a) as-anodized Ta–O and (b) that annealed up to 1058 K. Intensity of O K_α and S K_α normalized to that of Ta M_α is shown in the upper frame. (a') The BFI of the as-anodized nanotube corresponding to the profile (a) taken after beam-scanning. The arrow indicates a trace by beam-scanning.

B. Thermal analysis

Figure 5(a) shows a TG-DTA profile, obtained at a heating rate of 10 K/min in a stream of argon, of the amorphous Ta–O NTs. An endothermic peak appears at around 1100 K, where the weight of the sample, 21.7 mg, decreased by 2.2 mg. The simultaneously obtained thermal desorption spectra, shown in Fig. 5(b), indicate desorption of molecules of specific mass of 16, 32, 48, and 64 in the same temperature range as the endothermic peak. At 3 K/min, the endothermic peak started at 1058 K and completed at 1128 K. The anodized samples were subjected to heating in the TG-DTA instrument up to 1058 and 1128 K, respectively, and then furnace-cooled to ambient temperature. The results of XRD and TEM analyses, shown in Figs. 1–4 and 6, were obtained from those samples. The molecular species detected at temperatures around 400 K must be C (12), H_2O (18), and CO_2 (44), which are all likely to come from the sample surface and/or the environment. As observed by EDS (Fig. 3), amorphous NTs contain impurity sulfur and excess oxygen. The molecules detected at the temperature of the endothermic reaction, of specific mass 16, 32, 48, and 64, are most probably related with excess oxygen and sulfur contained in the amorphous NTs, and are identified as O, O_2, SO, and SO_2, respectively. Transformation of a metastable amorphous solid to its crystalline counterpart is usually an exothermic reaction. The observed endothermic peak must be due to the removal of the oxygen and sulfur from the amorphous oxide; the loss of the chemical bonding energies associated with these extra constituents was probably larger in magnitude than the lowering of the enthalpy on the crystallization. This point is further discussed in Sec. III. E.

The enthalpy of the endothermic reaction was estimated from the enclosed area of the peak, obtained by DSC measurement at 5, 10, 20, and 30 K/min, to be 13.4 ± 0.9 kJ/mol of Ta_2O_5.

C. Composition of anodized amorphous Ta–O

From the results of the thermal and XRD analyses, the endothermic reaction that occurs at around 1073 K must be described as

$$Ta_2O_{5+x}S_y\,(\text{amorphous}) \rightarrow \beta\text{-}Ta_2O_5 + xO + yS - 13.4\ \text{kJ/mol} \quad (1)$$

The amount of extra oxygen, x, and impurity sulfur, y, can be evaluated from the weight reduction before and after the endothermic reaction in the TG measurement and

https://doi.org/10.1557/jmr.2014.44 Published online by Cambridge University Press

the intensities of characteristic x-rays of sulfur and oxygen measured by EDS. As the specific mass of oxygen, sulfur, and Ta_2O_5, are 16, 32, and 441.8 g/mol, respectively, x and y satisfy the following relation

$$(16x + 32y)/441.8 = m_d/m_c \quad (2)$$

where m_d and m_c are the total mass of desorbed oxygen and sulfur, and the mass of Ta_2O_5, respectively. The molar ratio of sulfur to total oxygen in the amorphous oxide is roughly estimated from the intensities of the characteristic x-rays in the EDS spectra to be 0.11, i.e.,

$$y/(5 + x) = 0.11 \quad (3)$$

From the TG measurement, m_d and m_c were obtained to be 2.2 and 19.5 mg, respectively. By using Eqs. (2) and (3), x and y are calculated to be 1.6 and 0.7, respectively; the composition of the amorphous Ta–O NTs is $Ta_2O_{6.6}S_{0.7}$.

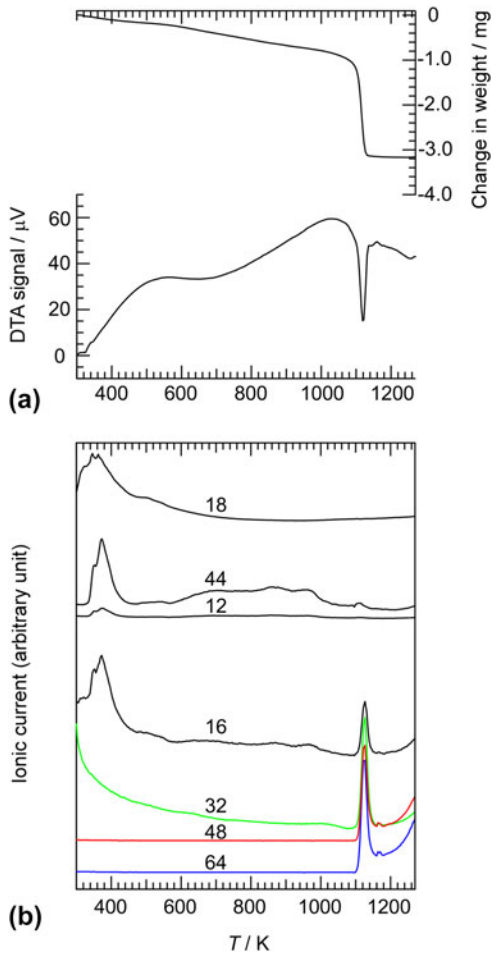


FIG. 5. (a) TG-DTA profile of anodic amorphous Ta–O NTs, measured at a heating rate of 10 K/min in a stream of high purity argon. (b) Simultaneously measured desorption curves. The number on each profile indicates the mass number of the detected species.

D. Pair distribution analysis

As mentioned earlier, the evolution of the broad maxima of the amorphous $Ta_2O_{6.6}S_{0.7}$ (a-$Ta_2O_{6.6}S_{0.7}$) in the XRD profiles [Figs. 1(a) and 1(b)] suggests structural changes during annealing. To characterize them quantitatively, the short-range atomic structures were evaluated in terms of RDFs by analyzing the selected-area electron diffraction patterns taken from a single NT in the electron beam of ~300 nm in diameter. To avoid contamination, electron diffraction intensities were measured at a cryogenic temperature using a cooling holder. From the recorded intensity profiles, reduced interference functions, $F(Q)$, were calculated. Here, Q is the scattering vector defined as $Q = 4\pi \sin\theta/\lambda$, where θ and λ are the scattering angle and the electron wavelength, respectively. The details of distribution function analysis using electron diffraction are described elsewhere.[18,19]

The atomic pair distribution function, $g(r)$ of a-$Ta_2O_{6.6}S_{0.7}$, extracted by the Fourier transform of $F(Q)$, is shown in Fig. 6(a). For comparison, $g(r)$ of an amorphous Ta_2O_5 (a-Ta_2O_5) prepared by sputtering[21] is shown in Fig. 6(b). Peaks appear at around 0.19, 0.27–0.28, 0.34, and 0.37 nm. It is known that the truncation of scattering vector (Q_{max}) in the reciprocal lattice space sometimes leads to spurious termination ripples, the so-called "ghost" peak, in RDFs.[22–24]

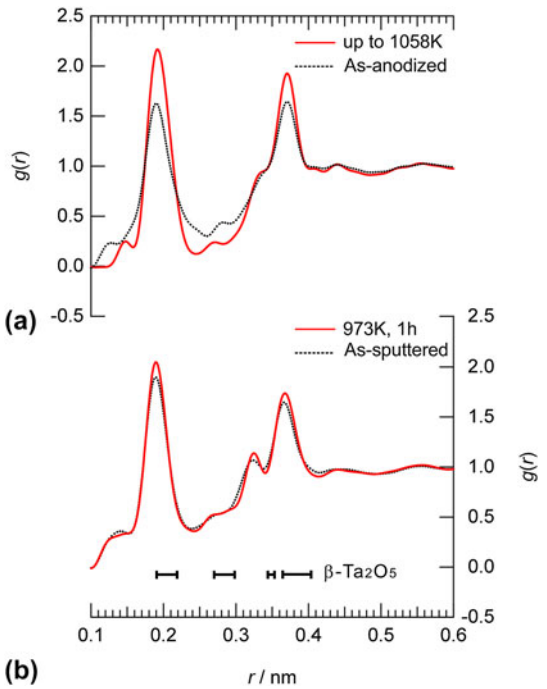


FIG. 6. Atomic pair distribution function $g(r)$ of (a) a-$Ta_2O_{6.6}S_{0.7}$ and (b) a-Ta_2O_5 prepared by sputtering.[21] Dotted black and red solid lines represent as-anodized (as-sputtered) and annealed samples, respectively. The experimental details for sputtered samples are in Refs. 17,21. $g(r)$ of annealed a-Ta_2O_5 is an original data for this publication.

https://doi.org/10.1557/jmr.2014.44 Published online by Cambridge University Press

We confirmed that the locations of the peaks and shoulders remain unchanged regardless of Q_{max}, suggesting that the peaks and shoulders discussed here are not ghost but real ones. These peaks are in good agreement with the bond lengths of Ta–O, O–O, Ta–Ta(1), and Ta–Ta(2), respectively (the number within the parentheses indicates the shorter and longer distance), in a-Ta_2O_5.[21,25] Therefore, the atomic distribution in a-$Ta_2O_{6.6}S_{0.7}$ prepared via anodization is essentially similar to that in a-Ta_2O_5. The bars at the bottom of Fig. 6(b) indicate the bond-length ranges of Ta–O, O–O, Ta–Ta(1), and Ta–Ta(2) in crystalline β-Ta_2O_5 (a = 0.389 nm, b = 4.029 nm, c = 0.620 nm[20]). The bond-lengths in its large unit cell are widely distributed and are located at longer distances than in the amorphous structure.

Although the peak intensity for Ta–O, Ta–Ta(1), and Ta–Ta(2) bonds increases slightly by annealing, $g(r)$ of annealed a-Ta_2O_5 is almost consistent with that of as-deposited a-Ta_2O_5. This tendency is true for amorphous transition-metal oxides such as Al_2O_3,[26] WO_3, and Nb_2O_5 (R. Nakamura et al., to be submitted). It is evident, on the other hand, that $g(r)$ of the annealed a-$Ta_2O_{6.6}S_{0.7}$ differs clearly from that of the as-anodized one. A notable feature is that the broad peak in $g(r)$ corresponding to Ta–O and Ta–Ta(2) in the as-anodized state becomes sharper by annealing. A considerable amount of sulfur, whose concentration is 7.5 at.%, is contained in the NTs. Thus, sulfur-related configurations such as Ta–S or O–S probably exist. In fact, the distance between Ta and S is known to be around 0.24 nm in the stable phase of tantalum sulfide, TaS_2, and in related compounds.[27–29] In addition, a large amount of excess oxygen may be located at positions deviating from the Ta–O configuration around 0.19 nm; excess oxygen may contribute to the broadening of the Ta–O peak. It is probable, therefore, that the shoulder at 0.24 nm of the as-anodized sample is due to Ta–S and Ta–O bonds, and their bond length becomes closer to that of the distribution around 0.19 nm as a result of atomic rearrangements at elevated temperatures. As can be seen in the partial pair distribution function of Ta–O bonds in a-Ta_2O_5,[25] the correlation corresponding to the second nearest Ta–O bonds appears weakly around 0.38 nm, which is close to the peak position of Ta–Ta(2). In the case of a-$Ta_2O_{6.6}S_{0.7}$ with higher concentration of oxygen than a-Ta_2O_5, the correlation of the second nearest Ta–O bonds is expected to be stronger and appear near the Ta–Ta(2) peak. The rearrangement of oxygen and sulfur by annealing makes the peak intensity for not only Ta–O but also Ta–Ta (2) increase. This can be interpreted as a unique structural change, which occurs owing to excess oxygen and sulfur. Radial distribution analysis revealed that excess oxygen and sulfur are introduced with a variety of bond lengths around Ta cations by the anodization process and then are rearranged by annealing toward a regular amorphous structure.

E. Origin of the thermal stability

Amorphous Ta_2O_5 thin films prepared by sputtering start to crystallize at 973 K and fully crystallize at 1023 K in 1 h in air.[17] With the same heat treatment, the amorphous structure of the a-$Ta_2O_{6.6}S_{0.7}$ was confirmed to be maintained by XRD measurements; in terms of the crystallization temperature, a-$Ta_2O_{6.6}S_{0.7}$ NTs are more stable than a-Ta_2O_5 films. The stabilization is most probably due to the presence of excess oxygen and impurity sulfur introduced in the anodization process.

The transformation of the anodically fabricated oxide to the stoichiometric crystalline phase by annealing is schematically illustrated in Fig. 7, including some hypothetical states, with the changes in enthalpy. The oxide contains excess oxygen and impurity sulfur in the as-prepared state (I). By annealing at around 1073 K, it releases extra oxygen and sulfur and crystallizes into stoichiometric β-Ta_2O_5 (IV), whose enthalpy is higher than the initial state by 13.4 kJ/mol. For convenience, we consider two hypothetical states, II and III, between them. First, the extra oxygen and sulfur are removed from state I (II), and next, the volume of the material is reduced, by eliminating the vacancies, to be the same as the ordinary stoichiometric amorphous oxide (III). The enthalpy is raised in state II by the loss of chemical bonds associated with the extra constituents. It is compensated to some extent in III (by elimination of vacancies) and IV (by crystallization), but not fully to the original level, leaving 13.4 kJ/mol, which was observed in the DSC. The oxygen and sulfur atoms released from the oxide must form stable molecules such as O_2, SO, and SO_2, as observed by mass spectroscopy, and leave the sample cell (state V). Since the sum of the heats of formation of those molecules is estimated to be at least 400 kJ/mol, the enthalpy of the final state (V) is far lower than the initial state (I) so that reaction (1) proceeds inevitably and irreversibly. (If all the excess O of 1.6 mol form O_2 molecules of 0.8 mol, the heat of formation amounts to -494 kJ/mol × 0.8 mol = -400 kJ/mol of Ta_2O_5.)

The enthalpy difference between a-$Ta_2O_{6.6}S_{0.7}$ and a-Ta_2O_5, H_{III} is due to chemical bonds by the extra oxygen and impurity sulfur. The difference between H_{III} and H_{IV}, i.e., crystallization enthalpy, ΔH_x, of a-Ta_2O_5, is unknown. Here, we assume it to be of similar magnitude to the crystallization enthalpy of other amorphous oxides, TiO_2, Nb_2O_5, and Al_2O_3, which is in the range of 17–40 kJ/mol.[30–32] With this assumption, the decrease in enthalpy of a-Ta_2O_5 per an extra atom is estimated to be 0.16–0.23 eV, which is a few percent of the bond energy, or the cohesive energy of a-Ta_2O_5, 5.34 eV.[33] (Decrease in enthalpy (per mole of Ta_2O_5) per mole extra atoms (1.6 mol of O and 0.7 mol of S) is (ΔH_x + 13.4 kJ/mol)/2.3 mol = 13.2−23.2 kJ/mol = 0.16 − 0.23 eV.)

https://doi.org/10.1557/jmr.2014.44 Published online by Cambridge University Press

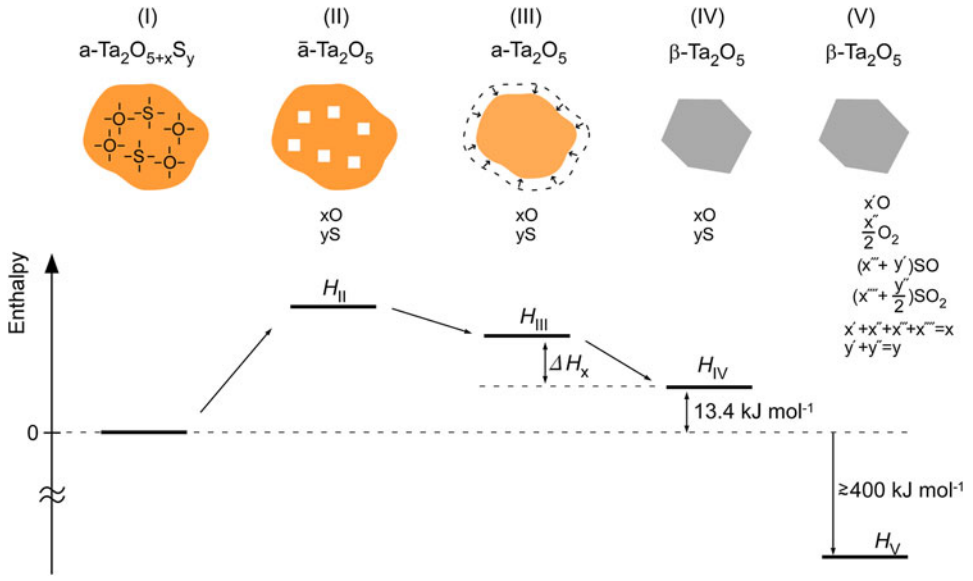


FIG. 7. Schematic diagrams for enthalpy at various stages of transformation, including hypothetical states: (I) a-$Ta_2O_{6.6}S_{0.7}$, (II, III) amorphous Ta_2O_5, and (IV, V) β-Ta_2O_5. State II contains an extra volume due to the removal of extra oxygen and sulfur from a-$Ta_2O_{6.6}S_{0.7}$. State V includes released molecules consisting of excess oxygen and sulfur.

Both the enthalpy and entropy of a-Ta_2O_5 (state III), which corresponds to a-Ta_2O_5 prepared by sputtering, are higher than those of crystalline β-Ta_2O_5 (state IV), and so is the free energy. For a-Ta_2O_5, therefore, the driving force of crystallization, that is the difference in free energy, must be negative. In contrast, it turned out that the enthalpy of a-$Ta_2O_{6.6}S_{0.7}$ (I) is 13.4 kJ/mol lower than that of β-Ta_2O_5 (IV), as discussed above, while the entropy of a-$Ta_2O_{6.6}S_{0.7}$ must be higher than that of β-Ta_2O_5. As a result, the free energy of a-$Ta_2O_{6.6}S_{0.7}$ is apparently lower than that of β-Ta_2O_5 (IV). However, the free energy of a-$Ta_2O_{6.6}S_{0.7}$ is far higher than that of β-Ta_2O_5 with desorbed molecules (V). Therefore, a-$Ta_2O_{6.6}S_{0.7}$ is not thermodynamically stabilized. The desorption of impurity sulfur and excess oxygen, which occurs simultaneously with the crystallization, rather indicates that the transformation is kinetically limited. For reaction (1) to proceed, impurity sulfur and excess oxygen are to be released from the amorphous solid, which is possible only at temperatures where atomic mobilities are high enough. At such high temperatures, the extra atoms diffuse out, leaving the composition of the solid closer to stoichiometry, and then crystallization eventually occurs.

IV. SUMMARY AND CONCLUSIONS

Thermal stability of amorphous Ta–O NTs prepared by anodization in a sulfuric solution was studied by combining thermal and structural analyses.

Considerable amounts of excess oxygen and impurity sulfur are contained in the amorphous NTs, whose composition was determined to be a-$Ta_2O_{6.6}S_{0.7}$. Radial distribution function analysis revealed a unique structural change, which arises from the excess oxygen and sulfur; broad bond-length distribution for Ta–O (around 0.19 nm) and Ta–Ta (around 0.37 nm) of as-anodized a-$Ta_2O_{6.6}S_{0.7}$ sharpens with annealing. Broad distribution of bond length around Ta in the as-anodized a-$Ta_2O_{6.6}S_{0.7}$ is due to chemical bonds formed by excess oxygen and sulfur. The structural change with annealing is caused by the rearrangement of excess oxygen and sulfur.

Amorphous $Ta_2O_{6.6}S_{0.7}$ crystallizes into β-Ta_2O_5 simultaneously as the impurity sulfur and excess oxygen desorb at around 1073 K with a positive change in enthalpy of 13.4 kJ/mol. The observed enthalpy change is attributed to the loss of chemical bonds, Ta–O and Ta–S, under compensated by the lowering of enthalpy due to reduction in volume and crystallization. Amorphous $Ta_2O_{6.6}S_{0.7}$ NTs are more stable than stoichiometric amorphous Ta_2O_5, which crystallizes around 973 K. The stabilization is of kinetic origin; the crystallization begins to occur only when the out-diffusion of extra oxygen and impurity sulfur becomes possible.

ACKNOWLEDGMENTS

The author (RN) would like to thank Dr. S. Hayashi (AIST) for the measurement of TG-DTA with a mass spectrometer. He also shows his appreciation to Dr. H. Tsuchiya (Osaka University) and Dr. S. Semboshi (Tohoku University) for their useful advice on sample preparation and Mr. S. Ueno (Osaka Prefecture University) for supporting preliminary TG-DTA measurements. The TEM observations were carried out at the Comprehensive Analysis Center of Institute of Scientific and Industrial

https://doi.org/10.1557/jmr.2014.44 Published online by Cambridge University Press

Research, Osaka University. A portion of this study was performed under the inter-university cooperative research program of the IMR, Tohoku University. This work was financially supported by Grant-in-Aid for Young Scientists (B) (No. 24760574).

REFERENCES

1. C.T. Kresge, M.E. Leonowicz, W.J. Roth, J.C. Vartuli, and J.S. Beck: Ordered mesoporous molecular sieves synthesized by a liquid-crystal template mechanism. *Nature* **359**, 710 (1992).
2. S.A. Johnson, P.J. Ollivier, and T.E. Mallouk: Ordered mesoporous polymers of tunable pore size from colloidal silica templates. *Science* **283**, 963 (1999).
3. H. Masuda and K. Fukuda: Ordered metal nanohole arrays made by a two-step replication of honeycomb structures of anodic alumina. *Science* **268**, 1466 (1995).
4. D. Gong, C.A. Grimes, O.K. Varghese, W. Hu, R.S. Singh, Z. Chen, and E.C. Dickey: Titanium oxide nanotube arrays prepared by anodic oxidation. *J. Mater. Res.* **16**, 3331 (2001).
5. I. Sieber, H. Hildebrand, A. Friedrich, and P. Schmuki: Formation of self-organized niobium porous oxide on niobium. *Electrochem. Comm.* **7**, 97 (2005).
6. H. Tsuchiya, J.M. Macak, A. Ghicov, L. Taveira, and P. Schmuki: Self-organized porous TiO_2 and ZrO_2 produced by anodization. *Corr. Sci.* **47**, 3324 (2005).
7. H. Tsuchiya and P. Schmuki: Self-organized high aspect ratio porous hafnium oxide prepared by electrochemical anodization. *Electrochem. Comm.* **7**, 49 (2005).
8. H. Tsuchiya, J.M. Macak, I. Sieber, L. Taveira, A. Ghicov, K. Sirotna, and P. Schmuki: Self-organized porous WO_3 formed in NaF electrolytes. *Electrochem. Comm.* **7**, 295 (2005).
9. W. Wei, J.M. Macak, and P. Schmuki: High aspect ratio ordered nanoporous Ta_2O_5 films by anodization of Ta. *Electrochem. Comm.* **10**, 428 (2008).
10. I. Paramasivam, H. Jha, N. Liu, and P. Schmuki: A Review of photocatalysis using self-organized TiO_2 nanotubes and other ordered oxide nanostructures. *Small* **8**, 3073 (2012).
11. X. Chen, S. Shen, L. Guo, and S.S. Mao: Semiconductor-based photocatalytic hydrogen generation. *Chem. Rev.* **110**, 6503 (2010).
12. N.K. Allam, X.J. Feng, and C.A. Grimes: Self-assembled fabrication of vertically oriented Ta_2O_5 nanotube arrays, and membranes thereof, by one-step tantalum anodization. *Chem. Mater.* **20**, 6477 (2008).
13. X. Feng, T.J. LaTempa, J.I. Basham, G.K. Mor, O.K. Varghese, and C.A. Grimes: Ta_3N_5 nanotube arrays for visible light water photoelectrolysis. *Nano Lett.* **10**, 948 (2010).
14. J.E. Barton, C.L. Stender, P. Li, and T.W. Odom: Structural control of anodized tantalum oxide nanotubes. *J. Mater. Chem.* **19**, 4896 (2009).
15. R.V. Gonçalves, P. Migowski, H. Wender, D. Eberhardt, D.E. Weibel, F.v.C. Sonaglio, M.J.M. Zapata, J. Dupont, A.F. Feil, and S.R. Teixeira: Ta_2O_5 nanotubes obtained by anodization: Effect of thermal treatment on the photocatalytic activity for hydrogen production. *J. Phys. Chem. C* **116**, 14022 (2012).
16. N.K. Allam and M.A. El-Sayed: Photoelectrochemical water oxidation characteristics of anodically fabricated TiO_2 nanotube arrays: Structural and optical properties. *J. Phys. Chem. C* **114**, 12024 (2010).
17. R. Nakamura, K. Tanaka, M. Ishimaru, K. Sato, T.J. Konno, and H. Nakajima: Self-elongated growth of nanopores in annealed amorphous Ta_2O_5 films. *Scr. Mater.* **66**, 182 (2012).
18. Y. Hirotsu, M. Ishimaru, T. Ohkubo, T. Hanada, and M. Sugiyama: Application of nano-diffraction to local atomic distribution function analysis of amorphous materials. *J. Electron Microsc.* **50**, 435 (2001).
19. M. Ishimaru: Electron-beam radial distribution analysis of irradiation-induced amorphous SiC. *Nucl. Instrum. Methods Phys. Res., Sect. B* **250**, 309–314 (2006).
20. R.S. Roth, J.L. Waring, and H.S. Parker: Effect of oxide additions on the polymorphism of tantalum pentoxide. IV. The system Ta_2O_5-Ta_2WO_8. *J. Solid State Chem.* **2**, 445 (1970).
21. R. Nakamura, M. Ishimaru, K. Sato, K. Tanaka, H. Nakajima, and T.J. Konno: Formation of highly oriented nanopores via crystallization of amorphous Nb_2O_5 and Ta_2O_5. *J. Appl. Phys.* **114**, 124308 (2013).
22. Y. Waseda: *The Structure of Non-crystalline Materials* (McGraw-Hill, International Book Co, New York, 1980).
23. S.R. Elliott: *Physics of Amorphous Materials*, 2nd ed. (Longman Scientific & Technical, UK, 1990).
24. M. Ishimaru, Y. Zhang, and W.J. Weber: Ion-beam-induced chemical disorder in GaN. *J. Appl. Phys.* **106**, 053513 (2009).
25. R. Bassiri, K.B. Borisenko, D.J.H. Cockayne, J. Hough, I. MacLaren, and S. Rowan: Probing the atomic structure of amorphous Ta_2O_5 coatings. *Appl. Phys. Lett.* **98**, 031904 (2011).
26. R. Nakamura, M. Ishimaru, K. Sato, K. Tanaka, and H. Nakajima, and T.J. Konno: Enhancement of nanovoid formation in annealed amorphous Al_2O_3 including W. *J. Appl. Phys.* **114**, 124308 (2013).
27. F. Jellinek: The system tantalum-sulfur. *J. Less Common Met.* **4**, 9 (1962).
28. J. Mahy, G.A. Wiegers, F. van Bolhuis, A. Diedering, and R.J. Haange: X-ray and electron diffraction study of intercalates Ag_xTaS_2. *Phys. Status Solidi A* **107**, 873 (1988).
29. A. Suzuki, T. Yamashita, K. Matsui, and M. Doyama: Thermal and structural measurements of the mixed crystal 1T-$TaS_{2-x}Se_{1-x}$. *J. Phys. Soc. Jpn.* **57**, 1707 (1988).
30. H. Xie, Q. Zhang, T. Xi, J. Wang, and Y. Liu: Thermal analysis on nanosized TiO_2 prepared by hydrolysis. *Thermochim. Acta* **381**, 45 (2002).
31. S.E. Filippova and L.A. Reznitskii: The temperature and enthalpy of crystallization of amorphous niobium oxide. *Russian J. Inorganic Chem.* **46**, 1640 (2001).
32. M. Tane, S. Nakano, R. Nakamura, H. Ogi, M. Ishimaru, H. Kimizuka, and H. Nakajima: Nanovoid formation by change in amorphous structure through the annealing of amorphous Al_2O_3 thin films. *Acta Mater.* **59**, 4631 (2011).
33. A.G. Gad-Allah, H.A. Abd El-Rahman, and M.M. Abou-Romia: Influence of oxide bond energies on the kinetics of chemical dissolution of anodic oxides on valve metals. *J. Appl. Electrochem.* **18**, 532 (1988).

https://doi.org/10.1557/jmr.2014.44 Published online by Cambridge University Press